JOURNAL OF MAGNETIC RESONANCE **124,** 291–297 (1997)
ARTICLE NO. MN961014

# The Spatial Dependence of Spin-Echo Signals

RICHARD P. O. JONES,* GARETH A. MORRIS,† AND JOHN C. WATERTON‡

**Department of Molecular Biophysics and Biochemistry, Yale University Magnetic Resonance Centre, P.O. Box 208043, New Haven, Connecticut 06520-8043; †Department of Chemistry, University of Manchester, Oxford Road, Manchester M13 9PL, United Kingdom; and ‡Department of Cardiovascular and Musculoskeletal Research, Zeneca Pharmaceuticals, Alderley Park, Macclesfield, Cheshire SK10 4TG, United Kingdom*

Received December 18, 1995; revised September 23, 1996

**The signals in NMR spin echoes which are refocused by 90° pulses are spatially modulated. The spatial modulation is not normally observed in images or profiles obtained using Hahn or stimulated echoes, but may cause errors if the sample structure varies on the distance scale of the modulation. Localized spectra measured using stimulated echoes will also show errors under these conditions. Simple Fourier-transform arguments show that conditions which allow the modulation to become visible in an image or profile have the effect of introducing a second echo into the time-domain acquisition window. Phase cycling may be used to remove the spatial dependence of the signals.** 

## INTRODUCTION

NMR coherences which are refocused by 90° pulses are widely used in high-resolution spectroscopy, while stimulated echoes are often used in single-voxel localized spectroscopy (*st*imulated-*e*cho *a*cquisition *m*ode, STEAM) (*1, 2*) and in MRI (*3*). It is not always appreciated that the magnetization which contributes to such echoes is spatially modulated. This paper discusses the signal variation as a function of position for the Hahn (90°—TE/2—90°—TE/2) and stimulated-echo (90°—TE/2—90°—TM—90°—TE/2) pulse sequences (*4*). The direction along which modulation occurs is that of the net gradient which dephases spins during the first TE/2 period of each sequence; the wavelength of the modulation varies inversely with the time integral of this gradient. For pulses of constant phase, in the Hahn echo the measured signal shows a sinusoidal variation with position, and in the stimulated echo the variation is cosinusoidal.

This spatial modulation of magnetization (*5*) is not generally observed in experimental profiles and images obtained from Hahn or stimulated echoes. The purposes of this paper are to present a simple analysis of the time-domain acquisition window which enables the observation of spatial modulation in the frequency domain, to point out some potential problems caused by the spatial modulation, and to show how it may be either retained or canceled by the use of appropriate phase cycles.

## THEORY

Consider the effect of applying the three-pulse stimulated-echo sequence to a sample which, when placed in a magnetic field $B_0$ oriented along the **z** axis of a Cartesian axis system, has a total equilibrium **z** magnetization $M_0^{\text{tot}}$ distributed evenly along the sample length $L$ in the direction **s** [$M_0(s) = M_0^{\text{tot}}/L$]. For simplicity, perfect shimming is assumed, along with negligible relaxation and diffusion; the frequency of a rotating frame of reference is chosen so that the radiofrequency pulses are on resonance at the position $s = 0$. The effect of applying the first 90° pulse, followed by a linear magnetic-field gradient of magnitude $G_1$ along **s** for a time $t_1$, is to generate transverse magnetization $M_{xy}(s) = M_x(s) + iM_y(s)$ which dephases by an angle $\theta(s) = \gamma G_1 s t_1$ to form a spatial helix [see, for example, Ref. (*6*)] about the **s** axis:

$$M_{xy}(s) = -iM_0(s)\exp\{i\theta(s)\}. \quad [1]$$

The helix will have $N(L) = \gamma G_1 t_1 L/2\pi$ turns over the sample length $L$, and the pitch of the helix (and hence the wavelength of the spatial modulation of magnetization) is given by $\Delta s = (2\pi/\gamma G_1 t_1)$.

The second 90° pulse converts the spatial helix of transverse magnetization into transverse and longitudinal components that oscillate as a function of $s$. The components of magnetization after this pulse are

$$M_{xy}^{\text{H}}(s) = M_0(s)\sin\{\theta(s)\} \quad [2]$$

$$M_z^{\text{S}}(s) = -M_0(s)\cos\{\theta(s)\}. \quad [3]$$

The term $M_{xy}^{\text{H}}(s)$ will go on to form the Hahn echo, and $M_z^{\text{S}}(s)$ will form the stimulated echo. The sine modulation in [2] is equivalent to two counter-rotating complex exponential terms. If the gradient $G_1$ were reimposed after the second 90° pulse, one of the exponential terms would have the right sense to be refocused and form a Hahn echo (HE); the other term would continue to dephase, giving negligible observed signal under normal conditions, and may be termed the Hahn anti-echo (HAE). The echo and anti-echo terms



1090-7807/97 $25.00

are often referred to as N- and P-type signals, respectively, from the negative and positive signs of their apparent precession frequencies during the evolution period $t_1$ of 2D NMR experiments (*7, 8*).

The effect of the third 90° pulse on term [3] is to convert the longitudinal magnetization back to transverse magnetization,

$$M_{xy}^{S}(s) = iM_0(s)\cos\{\theta(s)\}. \qquad [4]$$

Similarly, the cosine modulation in [4] corresponds to two counter-rotating terms, one which can be refocused by a gradient $G_1$ to give the stimulated echo (STE), and one (the stimulated anti-echo, STAE) which continues to dephase. The magnetization that contributes to the Hahn and the stimulated echoes is thus not independent of position, but shows respectively a sine and a cosine modulation as a function of *s*. Changing the relative phases of the first two 90° pulses will change the phases of the two spatial modulations, but there will always be a 90° phase shift between the modulation for the Hahn echo and that for the stimulated echo.

If the area $G_1t_1$ of the gradient pulse is sufficiently great, there will be a large number of turns $N(L)$ of the helix along the sample, the spins may be regarded as having an isotropic distribution of phases (*4*), and there will be little or no net signal after the first gradient pulse. Edge effects can be neglected, and on average half of the magnetization of the sample will contribute to the Hahn-echo term and half to the stimulated echo. If, on the other hand, $G_1t_1$ is not large and there is insufficient dephasing of transverse magnetization following the first pulse, then the division of sample magnetization between the two echoes will be unequal, and will vary with gradient pulse area (*9*), offset from resonance, and RF pulse flip angle and phase (*10*). In this case, the chemical shift can cause amplitude modulation of STEAM spectra (*11*), and static-field inhomogeneities can cause ''shading'' in $T_2^*$-weighted images (*12, 13*).

It might seem reasonable to expect that imaging or profiling experiments using Hahn or stimulated echoes would show evidence of the spatial modulation of the echo signals. However, if a simple read gradient is applied during acquisition in order to generate a spatial profile of the signal, no such variation is seen. This is because the window of *k* space sampled when recording the echo is incomplete: only if a ''prefocusing'' negative gradient pulse is applied before acquisition does the modulation become visible (*5, 9, 11–13*).

Figure 1 shows a single-slice image, formed from stimulated echoes, acquired using a prefocusing negative gradient pulse; the spatial modulation of magnetization along the *x* axis is now clearly visible. The effect of the negative gradient pulse is to introduce a second echo into the time-domain acquisition window; it is the interference between the two echo signals which causes the modulation seen in the resulting image. The effect of the negative gradient pulse is to defocus further the N-type signal, and first to refocus (*14*) and then to overshoot and defocus the P-type signal. During acquisition under a positive read gradient, the P-type signal refocuses first, and then the N-type echo. In the absence of the negative gradient pulse, the P-type signal remains defocused during acquisition: it may be regarded as a ''virtual echo'' which lies before the read pulse.

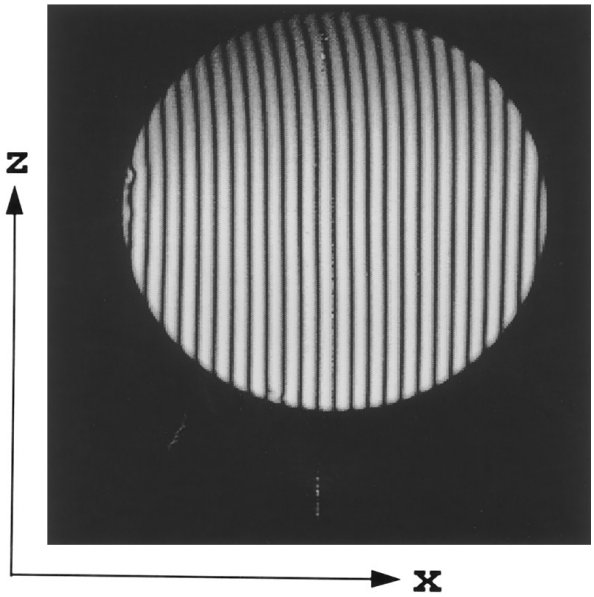


**FIG. 1.** A single-slice (thickness = 1 cm) image of a 10 cm diameter sphere containing water. The image was formed using the stimulated-echo pulse sequence as follows. The profiling gradient scheme of Fig. 2a was applied along the *x* axis. Phase-encoding gradients were applied along *z* after the third RF pulse. The two-step phase cycle 1 (Table 1) was used to remove artifacts while retaining the spatial modulation. With 256 phase-encoding steps, a total of 512 scans were acquired. A relaxation delay of 2.7 s resulted in a total image-acquisition time of 23 min. Other experimental parameters are described under Method.

The formation of the two echoes may be followed by considering the stimulated-echo signal-profiling pulse sequence of Fig. 2a, in which a prefocusing negative gradient pulse $-G_2$ of width $t_2$ is applied before the signal is acquired. Acquisition starts at time $t = 0$, under a read gradient $G_r$. During the acquisition, the magnetization $M_{xy}^{S}(s)$ evolves as

$$M_{xy}^{S}(s, t) = iM_0(s)\cos\{\theta(s)\}\exp\{i\phi(s, t)\}, \qquad [5]$$

where

$$\phi(s, t) = \gamma s(-G_2t_2 + G_rt). \qquad [6]$$

Integrating over *s* gives the time-domain signal for the entire sample:

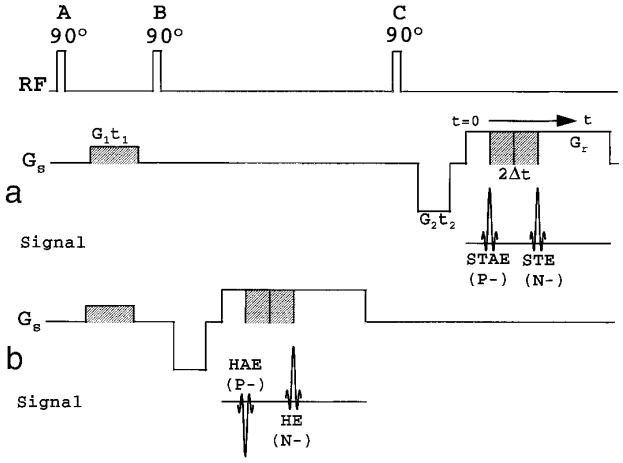


**FIG. 2.** Pulse-sequence and gradient schemes for the generation of (a) the stimulated echo (STE) and the stimulated anti-echo (STAE), and (b) the Hahn echo (HE) and the Hahn anti-echo (HAE).

$$M_{xy}^{S}(t) = \int_{-L/2}^{+L/2} M_{xy}^{S}(s, t)ds$$
$$= i\frac{M_0^{tot}}{2}\left[\frac{\sin\alpha}{\alpha} + \frac{\sin\beta}{\beta}\right], \qquad [7]$$

where

$$\alpha = \gamma\frac{L}{2}(G_r t - G_2 t_2 - G_1 t_1)$$
$$\beta = \gamma\frac{L}{2}(G_r t - G_2 t_2 + G_1 t_1). \qquad [8]$$

Setting $\alpha$ or $\beta$ to zero gives the conditions for maxima in Eq. [7], and two distinct echoes are predicted at times $t = \tau_1$ and $t = \tau_2$, respectively:

$$\tau_1 = (G_2 t_2 + G_1 t_1)/G_r$$
$$\tau_2 = (G_2 t_2 - G_1 t_1)/G_r. \qquad [9]$$

The stimulated echo occurs at $\tau_1$, while the stimulated anti-echo refocuses at $\tau_2$, a time $2\Delta t = 2G_1 t_1/G_r$ earlier. The spatial dependence of the echo signals at these times can be found by making the substitution $t = \tau_1$ or $\tau_2$ in Eq. [5]:

$$M_{xy}^{S}(s, \tau_1) = iM_0(s)\cos^2\{\theta(s)\}$$
$$- M_0(s)\cos\{\theta(s)\}\sin\{\theta(s)\}$$
$$M_{xy}^{S}(s, \tau_2) = iM_0(s)\cos^2\{\theta(s)\}$$
$$+ M_0(s)\cos\{\theta(s)\}\sin\{\theta(s)\}. \qquad [10]$$

The cosine-squared terms represent the partial refocusing of magnetization to form ''eight-ball'' echoes (*4*); the STE and the STAE have the same phase. Integration over *s* leads to the cancellation of the real terms in Eq. [10], leaving the pure imaginary result seen in [7].

The sine-modulated Hahn-echo term [2] can be treated in an analogous way using the gradient scheme of Fig. 2b, where the signal is acquired after the second pulse. The Hahn echo and Hahn anti-echo are observed at the same times $\tau_1$ and $\tau_2$. The sine modulation of magnetization leads to two ''eight-ball'' echoes which now consist of sine-squared terms, and which therefore have opposite phases (the anti-echo refocuses along the negative *y* axis).

In both cases, for a positive read gradient $G_r$ to refocus both the echo and anti-echo terms, a negative prefocusing gradient such that $|G_2 t_2| > |G_1 t_1|$ is required. For both echo maxima to fall within the acquisition time AQ, it is necessary that $|G_r \mathrm{AQ}| > |2G_1 t_1|$, which corresponds to the condition that the spatial resolution of the resulting image or profile be sufficient to resolve the modulation. As may be seen from Fig. 2, acquisition schemes which conform to these criteria are analogous to simple gradient-echo imaging sequences.

Simple Fourier-transform arguments show how the inherent spatial modulation of signal is masked on transformation of a single echo (Fig. 3a). For simplicity, the acquisition window in the time domain is assumed to be centered midway between $\tau_1$ and $\tau_2$. The echo, whether Hahn or stimulated, transforms to a signal profile in which the imaginary part shows a cosine dependence on frequency and the real part a sine dependence. The signal profile thus has a constant magnitude as a function of frequency (since $\sin^2\theta + \cos^2\theta = 1$), but is phase modulated with a periodicity of $1/\Delta t$ hertz. Since the frequency domain in such a one-dimensional profiling experiment corresponds to the spatial dimension,

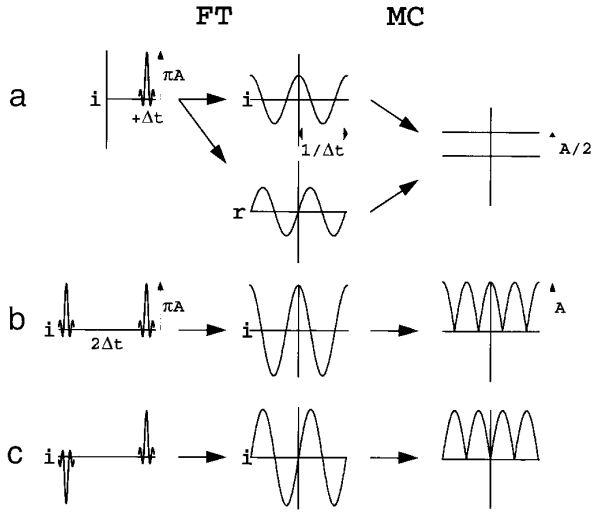


**FIG. 3.** Illustrations of Fourier-transform arguments for the appearance of spatial modulation, as described in the text.

with distance $s$ related to frequency $f$ through the expression $s = 2\pi f/\gamma G_r$, the spatial wavelength $\Delta s$ of the phase modulation is $2\pi/\gamma G_r \Delta t = 2\pi/\gamma G_1 t_1$, as seen earlier. If a prefocusing gradient pulse $-G_2$ is used to allow both echo signals to be acquired, the result of Fourier transformation is a pure imaginary signal with a cosine dependence on frequency or position if the echoes have the same phase (Fig. 3b), as in the stimulated-echo experiment, or a sine dependence if they are in antiphase (Fig. 3c), as in the Hahn-echo experiment. In both cases the signal magnitude profiles show modulation, which may be regarded as the interference pattern produced by the two echoes (*15*).

Simple phase cycles may be used to choose whether to retain the spatial modulation of magnetization when it is of use, or to cancel it when it may cause problems. Consider the stimulated-echo sequence of Fig. 2a. Changing the relative phases of the first two pulses A and B by 90° has two effects: the phase of the spatial modulation of stimulated-echo magnetization changes from a cosine to a sine function of $s$, and the relative phases of the STE and STAE change from being in-phase to being in antiphase. Hence, the $\cos^2\{\theta(s)\}$ refocused terms of Eq. [10] change to $\sin^2\{\theta(s)\}$ for the STE and to $-\sin^2\{\theta(s)\}$ for the STAE. Adding the signals obtained with the basic sequence of Fig. 2a and with a sequence where the phase of pulse B is shifted by ±90° relative to A allows the P- and N-type signals to be distinguished, as is done routinely in many 2D NMR spectroscopy experiments to allow $f_1$ quadrature detection. Changing the phase of the read pulse C, on the other hand, merely changes the axis along which the magnetization refocuses.

One obvious problem with the basic sequence of Fig. 2a is that a free-induction decay, generated by the third pulse (FID C), will appear in the acquisition window as a gradient echo, midway between the echo and the anti-echo. Phase cycle 1 (PC1, Table 1) cancels FID C but retains both echoes, hence retaining the spatial modulation. Phase cycle 2 (PC2, Table 2) cancels the spatial modulation of the summed signal by selecting only the (N-type) STE, and rejecting the (P-type) STAE, in the first two steps. Since alternate scans coadd STEs which have the form $M_0(s)\cos^2\{\theta(s)\}$ and $M_0(s)\sin^2\{\theta(s)\}$, their sum is $M_0(s)$, and the spatial modulation is removed. STAEs in alternate scans sum to a magnitude $M_0(s)[\cos^2\{\theta(s)\} - \sin^2\{\theta(s)\}]$, the integral of which

**TABLE 1**
**Phase Cycle 1 (PC1) for the Sequence of Fig. 2a to Retain the Spatial Modulation of Magnetization and to Remove FID C**

| $\phi_A$ | $\phi_B$ | $\phi_C$ | $\phi_R$ |
|---|---|---|---|
| 0 | 0 | 0 | 0 |
| 2 | 0 | 0 | 2 |

*Note.* $\phi_A$, $\phi_B$, and $\phi_C$ indicate the phases of the first, second, and third pulses, respectively, and $\phi_R$ indicates the receiver phase. Phase shifts are indicated as multiples of 90°: 0 for 0°, 1 for 90°, 2 for 180°, and 3 for 270°.

**TABLE 2**
**Phase Cycle 2 (PC2) for the Sequence of Fig. 2a to Cancel the Spatial Modulation of the Stimulated-Echo Signal and to Remove FID C**

| $\phi_A$ | $\phi_B$ | $\phi_C$ | $\phi_R$ |
|---|---|---|---|
| 0 | 0 | 0 | 0 |
| 0 | 1 | 0 | 1 |
| 2 | 0 | 0 | 2 |
| 2 | 1 | 0 | 3 |

*Note.* Symbols used are defined in the footnote to Table 1.

over $s$ is zero. The full four-step cycle also cancels FID C. Variations on phase cycle 2 have previously been used to cancel the modulation of signals by the chemical shift (*16, 17*). Full CYCLOPS (*18*) cycling of the phases of the receiver and all three pulses would extend the cycle to 16 scans.

Phase cycles 1 and 2 are purely illustrative; full cycles would include the suppression of unwanted coherence-transfer pathways and the compensation of pulse and receiver phase errors, extending the full cycles to 64 and 32 scans, respectively. Such phase cycles are in common use for the NOESY experiment, which uses the same pulse sequence [see, for example, Ref. (*19*)]; retention of both STE and STAE (and hence of spatial modulation of the acquired signal) corresponds to one or other of the two half phase cycles for hypercomplex phase-sensitive NOESY, while selection of either the STE or the STAE (suppressing modulation) corresponds to N- or P-type phase cycling, respectively, for the absolute-value NOESY experiment.

For spatial modulation to be observable in Hahn- or stimulated-echo images and profiles of a sample, certain conditions should be met. For image acquisition, the direction of the modulation must lie within the image plane; phase-encoding gradients during the first TE/2 period should be avoided, so that the direction and wavelength of modulation do not vary with the phase-encoding gradient. For spatial modulation to be seen in profiles, the direction of the modulation must coincide with the read gradient axis. Projection onto the read axis of magnetization which is modulated along a perpendicular direction would result in a profile of constant intensity. As a consequence, any dephasing of spins along the perpendicular directions during the first TE/2 period, for example, through the application of slice-selection gradients, must be refocused within this period.

## METHOD

A clinical research system consisting of a Bruker Biospec with an Oxford Instruments 2.1 T 1 m bore magnet was used. Profiling and imaging experiments were performed on a 10 cm diameter sphere containing water, placed in a volume coil. Stimulated echoes were generated using three 90° sinc pulses of 5 ms duration and 1200 Hz bandwidth. The gradient scheme of Fig. 2a was applied to obtain profiles along the $x$ axis. A 10 mm thick $xz$ plane was selected: pulse A was made slice selective to minimize spatial modulation of magnetization along $y$ due to field inhomogeneities; pulse C was made slice selective to minimize the transverse magnetization which originates solely from this pulse. A spoiler gradient was applied along the $z$ axis during TM to destroy all unwanted coherences (except for FID C) associated with the stimulated-echo sequence. A read gradient of 1000 Hz/cm and a spectral width of 13000 Hz gave a 13 cm field of view. The acquisition of 256 complex points ensured a high resolution of 0.05 cm per point. The dephasing product $G_1t_1$ was made large enough so that $N(L) \gg 1$, but small enough so that the wavelength of modulation, $\Delta s = 0.8$ cm, was much greater than the resolution. The product $G_2t_2$ was calculated as described previously, and adjusted so that the STE formed approximately at the center of the acquisition window, with the STAE preceding it.

## SIMULATIONS AND RESULTS

Figure 4a shows a computer simulation of the time-domain signal which would be obtained if the pulse sequence with the experimental parameters described above were applied to a 10 cm long sample of uniform magnetization. The simulation was obtained through numerical integration of Eq. [5] over 1000 isochromats along the sample length, for time increments across the acquisition window which corresponded to the experimental dwell time. It was assumed that the center of the sample was on resonance, and the gradients oriented along the long axis of the sample. Simultaneous sampling of the real and imaginary channels was simulated. The simulation demonstrates the refocusing of the STAE and STE in the imaginary (i) channel, with no signal in the real (r) channel. The echoes occur at the times predicted from the input parameters and Eqs. [9]; their separation $2\Delta t$ is 2.5 ms. Figure 4e, the magnitude calculation of the complex Fourier transform of the simulated time-domain signal, shows the spatial modulation of signal along the sample, with the predicted period.

In the experiments, sequential acquisition of real and imaginary points was used in measuring time-domain data; magnitude calculations (m) of the signals obtained are shown in Fig. 4. The experimental phantom used was spherical, as opposed to the one-dimensional sample used in the simulation, leading to the differences seen between the simulated and experimental envelopes of the echoes and profiles. Figure 4b shows the time-domain signal obtained with one scan of the pulse sequence described. The positions and separation of the STAE and STE agree with the simulation. The experimental difference in amplitude between the STAE and the STE arises from $B_0$ field inhomogeneity: the effects of inhomogeneity are refocused in the STE, giving $T_2$ weighting only, whereas they are not refocused in the STAE, giving $T_2^*$ weighting (*12*). The effect on the profile is to reduce the depth of the modulation slightly. Fourier transformation of the signal of Fig. 4b gives Fig. 4f, with the predicted spatial modulation seen in the profile of the sphere. Artifacts visible in Fig. 4b include the gradient echo, FID C, which bisects the two stimulated echoes and introduces a slight periodic distortion into the profile, and the large DC offset, which Fourier transforms to the spike at 0 Hz. As is shown by Figs. 4c and 4g, phase cycle 1 retains both echoes while removing the artifacts. Figure 4d illustrates the use of phase cycle 2 to remove the spatial modulation of magnetization.

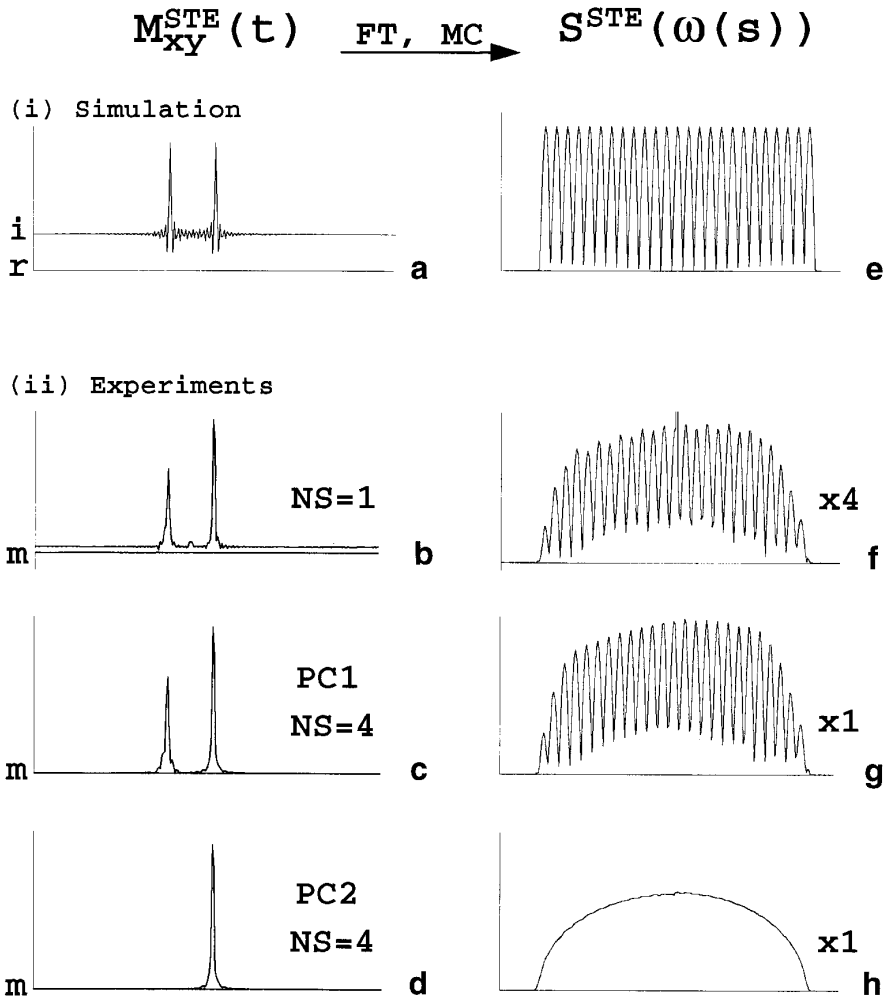


**FIG. 4.** (a)–(d) Time-domain signals associated with stimulated-echo magnetization, and (e)–(h) the corresponding magnitude spectra, as described in text, obtained (i) by numerical simulation and (ii) by using the experimental techniques described under Method. NS indicates the number of scans, while PC1 and PC2 indicate the use of the phase cycles of Table 1 and Table 2, respectively.

An STE of the same amplitude as in Fig. 4c is observed, but the STAE has been canceled. Fourier transformation gives the profile Fig. 4h, with approximately half of the peak magnitude of Fig. 4g.

## DISCUSSION

Hahn and stimulated echoes have been used extensively in both high-resolution and *in vivo* NMR spectroscopy. There has, however, been relatively little discussion of the spatial dependence of the magnetization which contributes to such echoes. One exception is the work of Axel and Dougherty on the SPAMM experiment (*5*), which exploits spatial modulation to label the magnetization of heart tissue so that its motion can be followed. Improved SPAMM pulse sequences have recently been used for myocardial motion tracking (*20, 21*). Problems caused by the long acquisition times needed to achieve high spatial resolution can be avoided if an echo-planar imaging sequence (*22*) is used following the SPAMM sequence, allowing single-shot imaging (*23*). Another example of the description of spatial modulation (for the Hahn echo) is Ref. (*6*), which analyzes the phenomenon of homonuclear multiple-spin echoes (MSEs). The modulation is absent for the heteronucleus in the heteronuclear multiple-spin-echo (HMSE) experiment (*24*) since a 90° pulse, rather than a Hahn-echo sequence, is used to excite the transverse heteronucleus magnetization.

Many imaging experiments use the Carr–Purcell sequence (*25*) to generate a spin echo, while spatial localization using the double-spin-echo technique PRESS (*26, 27*) is often compared (*28*) to that obtained using stimulated echoes (*1, 2*). Because the Carr–Purcell and PRESS experiments use 180° refocusing pulses, the resulting echoes do not show the spatial modulation described here.

The spatial modulation of spin-echo signals has a wide variety of potential applications, which have been outlined by Axel and Dougherty (*5*). However, spatial modulation may also have undesirable consequences for NMR experiments where HEs or STEs are acquired, whether the experiment be to obtain a profile or an image of the sample, or to obtain a spectrum from a localized volume (*1, 2*). First, the uncritical use of gradient pulses can lead to the unwanted appearance of spatial modulation in a profile or image. Second, and more important, the signals seen in Hahn and stimulated echoes vary rapidly with position, and hence may not be representative of a selected sample volume. The fact that this modulation is, in normal circumstances, masked from the experimenter can make it insidious: whether the modulation is visible or not, the signal measured still shows a periodic weighting as a function of position in the slice or voxel. If a sample contains structures which are of a dimension comparable to, or smaller than, the periodicity of the spatial modulation, then their contribution to the measured signal will change markedly depending on whether they lie close to a maximum or a minimum of the modulation pattern. In most applications this is unlikely to matter, but there are situations where the effects could be substantial. These include imaging of samples with strong periodicities, such as compact lamellar bone or skeletal muscle, microimaging of xylem in plants, angiography, and measurements of edge effects in imaging. Quantitative studies using difference methods would be particularly vulnerable, for example, the use of STEAM-localized water-signal measurement to follow function; not only would the sensitivity of an experiment to, say, a change in blood flow in a capillary depend on its exact position, but also very slight movements between scans could lead to large changes in the effects observed.

## ACKNOWLEDGMENTS

This work was supported by the National Institutes of Health (U.S. Public Health Service Grant DK34576). R.P.O.J. is most grateful to Professor R. G. Shulman for encouragement and instrument time, and acknowledges useful discussions with Dr. A. Blamire and Dr. D. L. Rothman.

## REFERENCES

1. J. Frahm, K.-D. Merboldt, and W. Hänicke, *J. Magn. Reson.* **72,** 502 (1987).
2. R. Kimmich and D. Hoepfel, *J. Magn. Reson.* **72,** 379 (1987).
3. J. Frahm, K.-D. Merboldt, W. Hänicke, and A. Haase, *J. Magn. Reson.* **64,** 81 (1985).
4. E. Hahn, *Phys. Rev.* **80,** 580 (1950).
5. L. Axel and L. Dougherty, *Radiology* **171,** 841 (1989).
6. R. P. O. Jones, G. A. Morris, and J. C. Waterton, *J. Magn. Reson.* **98,** 115 (1992).
7. R. Freeman, ''A Handbook of NMR,'' p. 111, Longman Scientific and Technical, Harlow, 1986.
8. J. Keeler and D. Neuhaus, *J. Magn. Reson.* **63,** 454 (1985).
9. D. Ballon, M. Garwood, and J. A. Koutcher, *Magn. Reson. Imaging* **9,** 569 (1991).
10. J. Frahm, H. Bruhn, M. L. Gyngell, K. D. Merboldt, W. Hänicke, and R. Sauter, *Magn. Reson. Med.* **9,** 79 (1989).
11. W. Zhang and P. Van Hecke, *J. Magn. Reson.* **91,** 408 (1991).
12. W. Zhang, *Magn. Reson. Med.* **32,** 230 (1994).
13. P. Bendel, *Magn. Reson. Med.* **30,** 399 (1993).
14. R. J. Ordidge, S. Punwani, and J. Thornton, Abstracts of the Society of Magnetic Resonance in Medicine, 3rd Annual Meeting, p. 670, 1995.
15. J. Hennig, *J. Magn. Reson.* **16,** 390 (1990).
16. L. Bolinger, R. E. Lenkinski, and J. S. Leigh, Abstracts of the Society of Magnetic Resonance in Medicine, 9th Annual Meeting, p. 1330, 1990.
17. P. B. Kingsley and J. S. Taylor, Abstracts of the Society of Magnetic Resonance in Medicine, 11th Annual Meeting, p. 3814, 1992.
18. D. I. Hoult and R. E. Richards, *Proc. R. Soc. (London) A* **344,** 311 (1975).
19. H. Kessler, M. Gehrke, and C. Griesinger, *Angew. Chem. Int. Ed. Engl.* **27,** 490 (1988).
20. S. E. Fischer, G. C. McKinnon, S. E. Maier, and P. Boesiger, *Magn. Reson. Med.* **30,** 191 (1993).
21. S. E. Fischer, G. C. McKinnon, M. B. Scheidegger, W. Prins, D. Maier, and P. Boesiger, *Magn. Reson. Med.* **31,** 401 (1994).
22. P. Mansfield, *J. Phys. C* **10,** L55 (1977).
23. P. Bornert and D. Jensen, Abstracts of the Society of Magnetic Resonance in Medicine, 12th Annual Meeting, p. 1235, 1993.
24. J. C. Waterton, R. P. O. Jones, and G. A. Morris, *J. Magn. Reson.* **97,** 218 (1992).
25. H. Y. Carr and E. M. Purcell, *Phys. Rev.* **94,** 630 (1954).
26. P. A. Bottomley, U.S. Patent 4 480 228 (1984).
27. R. J. Ordidge, M. R. Bendall, R. E. Gordon, and A. Connelly, ''Magnetic Resonance in Medicine and Biology,'' p. 387, McGraw–Hill, New York, 1985.
28. C. T. W. Moonen, M. von Kienlin, P. C. M. van Zijl, J. Cohen, J. Gillen, P. Daly, and G. Wolf, *NMR Biomed.* **2,** 201 (1989).